Indian Journal of Chemistry
Vol. 61, September 2022, pp. 928-942
DOI: 10.56042/ijc.v61i9.59413

Synthesis, structural, spectral and molecular docking of Ni(II) and Pd(II) complexes with isatin moiety and their DNA cleavage activity

Amna Q Ali*[a], Abdusalam M Hamil[a], Naser E Eltayeb*[b,c], Siang G Teoh[d], Saied M Soliman[e], Jamal Lasri[b] & Mostafa A Hussien[f,g]

[a] Chemistry Department, Faculty of Science, Sebha University, Sebha, Libya
[b] Department of Chemistry, Rabigh College of Science and Arts, P.O. Box 344, King Abdulaziz University, Jeddah, Saudi Arabia
[c] Department of Chemistry, Faculty of Pure and Applied Science, International University of Africa, Khartoum, Sudan
[d] School of Chemical Sciences, University Sains Malaysia, Minden-11800, Pulau Pinang, Malaysia
[e] Department of Chemistry, Faculty of Science, Alexandria University, P.O. Box 426, Ibrahimia, Alexandria 21321, Egypt
[f] Department of Chemistry, Faculty of Science, King Abdulaziz University, P.O. Box 80203 Jeddah 21589, Saudi Arabia
[g] Department of Chemistry, Faculty of Science, Port Said University, Port Said 42521, Egypt

E-mail: amn.abdalhafid@sebhau.edu.ly (AQA), netaha@kau.edu.sa (NEA)

Received 18 January 2022; accepted (revised) 18 July 2022

New complexes of Ni(II) and Pd(II) with Schiff base ligand derived from 5-nitro isatin with 4-phenyl-3-thiosemicarbazide have been synthesized in absolute ethanol. The isolated solid compounds have been characterized by elemental analyses and spectral (FT-IR, ^{1}H NMR and UV-Vis) measurements. The Schiff base ligand has been further characterized by single-crystal XRD. It has been found that the Schiff base ligand behaves as a tridentate ligand forming chelates with 1:2 (metal:ligand) in the case of Ni-complex and 1:1 (metal:ligand) in the case of Pd-complex. Octahedral geometry has been suggested for the Ni(II) chelate while square-planar geometry has been suggested for the Pd(II) chelate. The supramolecular structure of the thiosemicarbazide is controlled by large number of short intermolecular contacts such as O…H, H…H, C…C, S…C, S…H, S…N, H…C, N…O and C…O interactions where the most dominant contacts are H…H, H…C, C…C, O…H and S…H interactions. The optimized molecular geometry calculated at B3LYP/6-31G(d,p) level agreed very well with the reported X-ray structure. The two bands observed at 434 and 250 nm in the UV-Vis spectrum of the compound in DMSO as solvent have been calculated using TD-DFT method at 430.9 nm (f = 0.1178) and 257.2 nm (f = 0.387), respectively. These bands have been assigned to HOMO→LUMO (96%) and HOMO→LUMO+2 (90%) excitations which belong to n-π* and π-π* transitions, respectively. All the synthesized compounds have been tested against supercoiled pBR322 DNA. These compounds have been found to promote the cleavage of plasmid DNA in the presence of H_2O_2. The molecular docking of the ligand and its metal complexes refer to groove binding toward the DNA with high docking score of Ni(II) complex rather than the corresponding ligand and Pd(II) complex.

Keywords: 5-Nitro isatin, octahedral-geometry, 4-phenyl-3-thiosemicarbazid, single-crystal XRD, square-planar geometry, supercoiled pBR322

Isatin (indole-2,3-dione) moiety also known as indenedione and indole quinone is an important class of nitrogen-containing heterocyclic aromatic compounds found in the mammalian brain, plants, and human blood. Isatin was first isolated by Erdmann and Laurent as an oxidation product of indigo using nitric and chromic acids. Isatin and its derivatives possess a diverse array of potentially useful biological properties such as anticancer and antiviral, anticonvulsants, anti-bacterial and anti-fungal[1-5]. It is also used in traditional Chinese medicine for the treatment of a diversity of diseases caused by microorganisms and virus[6]. Similarly, the isatin-Schiff base complexes have established significant biological activity, including antitumor, antifungal, antiviral, antibacterial, and antimalarial agents[7,8]. The donor atoms such as nitrogen and oxygen/sulfur in the ligands play an important role in coordination with metal ions at the active sites of various large biomolecules. The nature of the ligands and the metals is important in the interaction of the coordination complexes with the DNA molecule. A huge number of coordination metal complexes have been found to promote DNA cleavage because of their redox properties[9,10]. The cleavage of the DNA can occur *via* a hydrolytic or oxidative pathway. The

hydrolytic pathway involves cleavage of the phosphodiester bond, which could be achieved by the enzymes; here, metal ions play a central role in mediating such cleavage pathway, while the oxidative cleavage includes nucleobase oxidation and/or degradation of sugar[11]. The current work describes the synthesis and spectroscopic characterization of nickel(II) and palladium(II) complexes with (*Z*)-2-(5-nitro-2-oxoindolin-3-ylidene)-*N*-phenylhydrazinecarbothioamide Schiff base. Single crystal X-ray structure of the Schiff base has been determined to confirm its structure. The nuclease activity with supercoiled pBR322 DNA activity of these compounds has been examined.

Materials and methods

Instrumentations

The materials used in this study such as 5-nitroisatin, 4-phenyl-3-thiosemicarbazide, nickel(II) chloride hexahydrate and palladium(II) chloride were purchased from Aldrich Chemicals. Commercial grade solvents and other reagents were used as supplied without further purification. Supercoiled (SC) pBR322 DNA and loading dye were purchased from Fermentas. Agarose (molecular biology grade), and ethidium bromide (EB) were purchased from Sigma (St. Louis, MO, USA). The elemental analyses were carried out using Perkin-Elmer 2400 series-11 CHN/O analyzer (Waltham, MA, USA). Infrared (IR), ultraviolet–visible (UV-Vis) and nuclear magnetic resonance (NMR) spectra were recorded, respectively, on Perkin Elmer 2000, Perkin Elmer-Lambda 25 and Bruker 500 MHz spectrometers at RT using DMSO-d_6 as the solvent and TMS as an internal standard.

Synthesis of Schiff base ligand [(*Z*)-2-(5-nitro-2-oxoindolin-3-ylidene)-*N*-phenylhydrazinecarbothioamide]

Schiff base ligand was synthesized by refluxing the ethanolic solution (30 mL) of 4-phenyl-3-thiosemicarbazide (0.01 mol) and 5-nitro isatin (0.01 mol) for 2 h. At the end of the reaction, the precipitates formed were filtered and washed with cold ethanol and finally stored in a vacuum desiccator over P_2O_5 (Scheme I).

$C_{15}H_{11}N_5O_3S$: Orange crystals; M.wt.: 341.06; MP: 239.2 to 240.6°C; Yield: 92%; analytical calculated values: C (52.78%), H (3.25%) and N (20.52%); analytical results (experimental): C (52.47%), H (3.30%) and N (20.75%); selected IR data (KBr pellet, υ_{max}/cm^{-1}): 3440 to 3077 (NH), 1693 (C=O), 1625 (C=N), 1593 (C=C) and 1212/765 (C=S) and ^{1}H NMR (500 MHz, DMSO-d_6) [δ (ppm)]: 12.67 (s, 1H, thiosemicarbazide N-N*H*), 11.26 (s, 1H, indole N-*H*), 10.85 (s, 1H, CS-N*H*), 7.63 to 7.61 (dd, 1H, indole C3-*H*, J_{HH} = 8.1 and 2.6 Hz), 7.60 (d, 2H, thiosemicarbazide C11-*H*, C15-*H*, J_{HH} = 7.79 Hz), 7.44 to 7.41 (t, 2H, thiosemicarbazide C12-*H*, C14-*H*, J = 7.78 Hz), 7.30 to 7.26 (t, 1H, thiosemicarbazide C13-*H*, J_{HH} = 7.38 Hz), 7.22 to 7.18 (dt, 1H, indole C5-*H*, J_{HH} = 7.7 and 2.5 Hz), 6.94 to 6.92 (dd, 1H, indole C2-*H*, J_{HH} = 8.6, and 4.1 Hz).

Synthesis of metal complexes

Synthesis of nickel(II) complex

The Schiff base nickel(II) complex was synthesized by refluxing the ethanolic solution (30 mL) of nickel(II) chloride ($NiCl_2.6H_2O$; 0.01 mol) and Schiff base ligand (0.02 mol) for 2 h. At the end of the reaction, the precipitate formed was filtered and washed with ethanol and finally stored in a vacuum desiccator over P_2O_5 (Scheme II).

$C_{30}H_{24}N_{10}NiO_8S_2$: Green powder; M.wt.: 775.40; MP: > 250°C; Yield: 85%; analytical calculated values: C (46.47%), H (3.12%), N (18.06%) and Ni (7.56%); analytical results (experimental): C (46.27%), H (3.10%), N (17.90%) and Ni (7.50%); selected IR data (KBr pellet, υ_{ma}/cm^{-1}): 3375 to 3062 (NH), 1661 (C=O), 1619 (C=N), 1599 (C=C) and 745 (C-S).

Synthesis of palladium(II) complex

The Schiff base palladium(II) complex was synthesized by refluxing the ethanolic solution (30 mL) of palladium(II) chloride ($PdCl_2$; 0.01 mol)

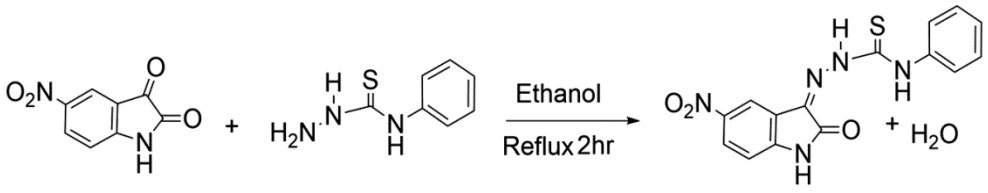

Scheme I — Synthesis of Schiff base ligand

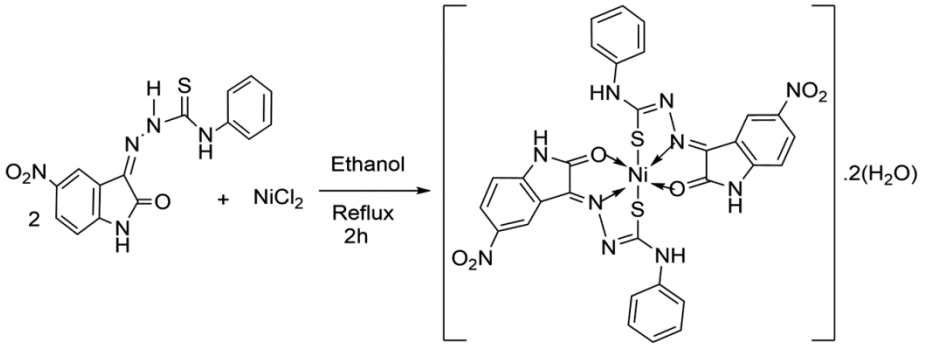

Scheme II — Synthesis of nickel(II) complex

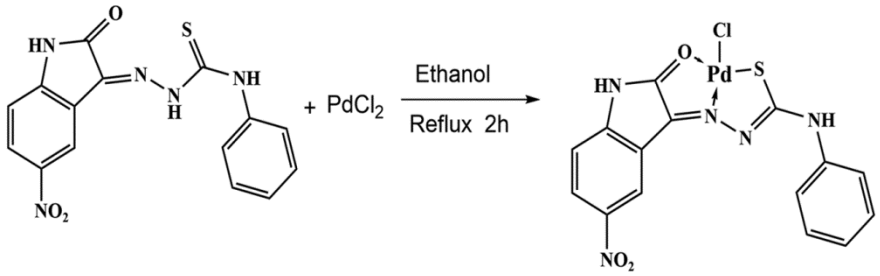

Scheme III — Synthesis of palladium(II) complex

and Schiff base ligand (0.01 mol) for 2 h. At the end of the reaction, the precipitate formed was filtered and washed with ethanol and finally stored in a vacuum desiccator over P_2O_5 (Scheme III).

$C_{15}H_{12}ClPdN_5O_3S$ (PdL): Brown powder; M.wt.: 482.94; MP: > 250°C; Yield: 85%; analytical calculated values: C (37.21%), H (2.50%), N (14.46%) and Pd (21.98%); analytical results (experimental): C (37.51%), H (2.47%), N (14.15%) and Pd (22.01%); selected IR data (KBr pellet, υ_{ma}/cm^{-1}): 3340 to 3055 (NH), 1647 (C=O), 1612 (C=N), 1600 (C=C) and 745 (C-S).

X-ray crystallography

The X-ray diffraction data was collected on a Bruker APEX II using Mo Kα radiation. The *Apex2*[12] program package was used for cell refinements and data reductions. Multi-scan absorption correction (*SADABS*)[12] was applied to the intensities before structure solution. The structures are solved by intrinsic phasing method using the *SHELXT*[13] software. Structural refinement is carried out using *SHELXL-2017*[13]. The crystallographic details are summarized in Table I.

The Cambridge Crystallographic Data Centre (CCDC) number 909979 contains the supplementary crystallographic data for this paper. These data can be obtained free of charge from CCDC *via* www.ccdc.cam.ac.uk/data_request/cif.

Table I — Crystal data and crystallographic refinement details.

Crystal system, space group	Monoclinic, *C*2/*c*
Temperature (K)	100
a, *b*, *c* (Å)	32.6902 (5), 21.3639 (3), 15.2582 (2)
β (°)	109.297 (1)
V (Å^3)	10057.5 (3)
Z	12
Radiation type	Mo *K*α
μ (mm^{-1})	0.23
Crystal size (mm)	0.43 × 0.22 × 0.19
Data collection	
Diffractometer	Bruker, APEXII
Absorption correction	Multi-Scan
No. of measured, independent and observed [$I > 2\sigma(I)$] reflections	74380, 18805, 13454
R_{int}	0.034
$(\sin\theta/\lambda)_{max}$ (Å^{-1})	0.765
Refinement	
$R[F^2 > 2\sigma(F^2)]$, $wR(F^2)$, S	0.066, 0.182, 1.02
No. of reflections	18805
No. of parameters	742
H-atom treatment	H atoms treated by a mixture of independent and constrained refinement $w = 1/[\sigma^2(F_o^2) + (0.079P)^2 + 23.650P]$ where $P = (F_o^2 + 2F_c^2)/3$
$\Delta\rho_{max}$, $\Delta\rho_{min}$ (e Å^{-3})	1.33, −0.79

Hirshfeld surface analysis

The topology analyses were performed using Crystal Explorer 17.5 program[14].

Computational methods

All DFT calculations were performed using Gaussian 09 software package[15] utilizing B3LYP/6-31G(d,p) method. Natural bond orbital analyses were performed using NBO 3.1 program as implemented in the Gaussian 09W package[16]. The self consistent reaction field (SCRF) method[17,18] was used to model the solvent effects when calculating the optimized geometries in solution. The structure was optimized in DMSO as solvent, then the electronic spectra were calculated using the time-dependent density functional theory (TD-DFT) and the results were used to assign the experimental UV-Vis spectra.

DNA cleavage studies

Cleavage experiments of supercoiled pBR322 DNA (0.5 μg/μL) were performed at *p*H 7.2 in Tris-HCl/NaCl (5:50 mM) buffer. Oxidative DNA cleavage was monitored by treating pBR322 DNA with varying concentrations of Schiff base ligand (1.0 to 6.0 mM) and Ni(II) or Pd(II) complexes (0.1 to 1 mM) and H_2O_2, followed by dilution with Tris-HCl/NaCl (5:50 mM) buffer to a total volume of 20 μL (Lanes 4 to 12). To investigate the mechanism of DNA cleavage promoted by these compounds, the experiment was carried out by adding scavenger for reactive oxygen species (ROS), DMSO to compound-DNA mixture (lane 3). The samples were incubated for 2 h at 37°C. A loading dye was added, and electrophoresis was carried out at 50 V for 1 h in Tris–HCl buffer using 1% agarose gel. The resulting bands were stained with EB before being photographed under UV light.

Molecular docking studies

Molecular docking studies were carried out using MOE 2019.0120 software by triangle matcher method. The refinement was performed by using rigid DNA and the docking score was calculated for the highest 30 by London dG and the best five scores were collected. The blind docking calculation was performed between the ligand and its metal complexes. The crystal structure for B type DNA "d(CGCAAATTTCGC)2" (PDB ID: 1BNA) is downloaded from protein data bank" https://www.rcsb.org/"[19]. The downloaded DNA was corrected and optimized for docking by removing all water molecules[20].

Results and Discussion

The nickel(II) and palladium(II) complexes were obtained in good yields from the reaction of nickel(II) or palladium(II) salt with Schiff base ligand in 1:2 or 1:1 (metal:ligand) ratio, respectively, under solvent reflux for 2 h.

Spectroscopic Study

IR studies

IR spectrum of Schiff base (Figure S1) exhibits absorption bands at 1693 and 1625 cm^{-1} and can be assigned to (C=O) and (C=N) respectively, which confirms the formation of the Schiff base product. The peak at 1593 cm^{-1} may be assigned to (C=C) as reported for similar compounds[21]. The peak at 1153 cm^{-1} results from υ(N-N) stretching vibration band. The Schiff base contains a thione group (C=S) with protons adjacent to it. Although, it has been noted that the thione group is relatively unstable in the monomeric form and tends to convert to a stable C–SH single bond. Absence of any bands in the 2800-2550 cm^{-1} region confirms the lack of —SH stretching frequencies in the molecule. It reveals the presence of only the thione tautomer in the solid state (bands at 1212 / 785 cm^{-1}). However, equilibrium with the thiolo tautomeric form may be recognized in solution[22].

The characteristic IR bands recorded for the free ligand differ from those of the related metal complexes and provided significant indications of the bonding sites of thiosemicarbazone ligand. In comparison with the spectrum of the Schiff base, the Ni and Pd complexes (Figures S2 and S3) exhibited the band of *ν*(C=O) within 1647–1671 cm^{-1}, showing a shift of the band to lower wavenumbers. This finding indicates that, the carbonyl oxygen is coordinated to the metal ion. The band of *ν*(C=N) within 1612–1619 cm^{-1} in the metal complexes show a shift of the band to lower wavenumbers, which indicates that the nitrogen atom of the azomethine group is coordinated to the metal ion. This finding is further supported by the band at 745 cm^{-1} in the metal complexes because of *ν*(C−S) [23]. Thus, the IR spectral results of the complexes provide supporting evidence for the complexation of Schiff base with metal ions in tridentate mode.

UV-Vis studies

The UV-Vis spectra of the complexes recorded in DMSO solution show similar pattern suggesting that

the complexes retain their structure in solution. The electronic spectrum of the free ligand (Figure S4) consists of an intense band centered at 434 nm attributed to n-π* transitions of the azomethine group. There is another intense band at 250 nm related to π-π* transitions of phenyl rings[24]. These transitions are also found in the spectra of the complexes, but they shifted to lower frequencies. The spectrum of nickel complex (Figure S5) showed two bands in visible region, 600 and 485 nm assigned to d-d transitions, typical for octahedral complexes[25].

The electronic spectrum of the palladium (II) complex (Figure S6) showed bands in the region 206-465 nm. The appearance of bands below 465 nm suggests a square planar geometry around the Pd(II) in the complex. The band at 255 nm has been assigned to intra ligand transitions and the band appearing at of 370 nm has been assigned to LMCT (S→d) transitions. The band at 465 nm is due to MLCT (metal to ligand charge transfer) [26].

^{1}H NMR study

The ^{1}H NMR spectrum of the ligand (Figure S7), which have a phenyl group at the thiosemicarbazide moiety, exhibit three separate singlets at δ 12.67, 11.26 and 10.85 ppm attributed to N-N*H* of thiosemicarbazide, indole N-*H* moiety and CS-N*H* proton of the thiosemicarbazide moiety, respectively, as reported previously for similar compounds[27]. The indole C2-*H* and C3-*H* appeared as a doublet at δ 7.63–6.93 ppm, while the indole C5-*H* appeared as a singlet at δ 7.50 ppm.

Crystal description

Three molecules of isatin crystallized with two dimethylformamide (DMF) molecules in the asymmetric unit as shown in Figure 1. In isatin molecules the dihedral angle between benzene ring in isatin (indoline-2,3-dione) moiety (C1-C6) and the benzene ring (C10–C15) are 7.83(10)°, 1.42(12)° and 11.14(11)° for isatin molecules A, B and C, respectively. The C=S bond has double bond nature as indicated by its bond length 1.662(2) Å. All C-N bonds have single bond character except C7=N2 which showed 1.298(2) Å bond length. The bond lengths and angles of the isatin moiety of title compound are also comparable with the values observed for related structures[28-30]. Selected bond lengths are depicted in Table II. In the crystal structure, these molecules are stablilized by intramolecular and intermolecular hydrogen bonds and the data are summarized in Table III.

Analysis of molecular packing

The Hirshfeld analysis is one of the simplest tool to investigate the molecular packing in the crystal structure both at the qualitative and quantitative levels[33-37]. The d_{norm} surfaces showing different regions contributed in short interactions with the neighboring molecules are shown in Figure 2.

The molecular packing is controlled by a large number of short intermolecular contacts such as O…H, H…H, C…C, S…C, S…H, S…N, H…C, N…O and C…O interactions. All these contacts appeared as red regions in the d_{norm} map. The crystal structure of the studied compound showed three molecular units in the asymmetric formula. They differ to some extent in the packing or intermolecular contacts with the neighboring molecular units. For example, there is no short H…H, S…C or H…C interactions could be observed in unit C while all these three contacts are found in units A and B with short contact distances. In addition, units A and C are

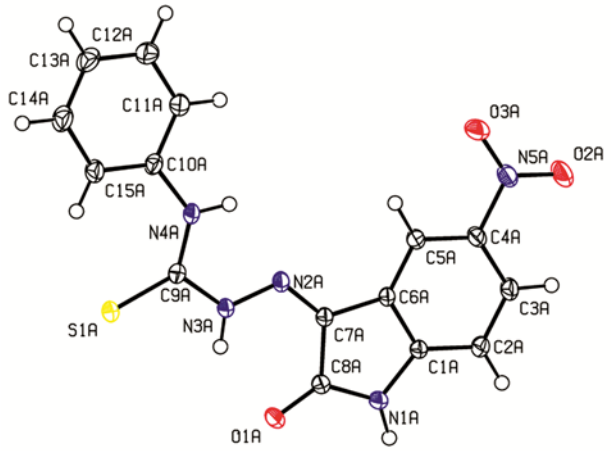

Figure 1 — A view of the structure of (l4_0m) (moiety $C_{15}H_{11}N_5O_3S$), showing the atom-labelling scheme. Displacement ellipsoids are drawn at the 50% probability level, solvent molecules and other two molecules are omitted for clarity.

Table II — Selected bond lengths (Å)

S1A—C9A	1.6667 (18)	N4B—C9B	1.337 (2)
N1A—C8A	1.364 (2)	N4B—C10B	1.422 (2)
N1A—C1A	1.402 (2)	S1C—C9C	1.6623 (19)
N2A—C7A	1.299 (2)	N1C—C8C	1.360 (3)
S1B—C9B	1.6617 (19)	N1C—C1C	1.402 (2)
N1B—C8B	1.366 (2)	N2C—C7C	1.295 (2)
N1B—C1B	1.401 (2)	N4C—C9C	1.342 (2)
N2B—C7B	1.298 (2)	N4C—C10C	1.416 (2)

packed together *via* significantly short π…π contacts (regions C), while unit B showed π…π stacking interactions at longer distances and are considered of less significance. The shortest C…C contact distance in unit B is 3.429 Å which is slightly longer than the van der Waals radii sum of two carbon atoms (3.40 Å). The corresponding distances in units A and B are in the range of 3.228-3.359 Å. Similarly, units A and C are involved in some S…H interactions which is not found in case of unit B (Figure 2). Summary of all possible short contacts and the corresponding interaction distances are listed in Table IV. This table comprised all intermolecular interactions with short contact distances which appeared as red regions in the d_{norm} map. Hence, those represent only the contacts with shorter distances than the van der Waals radii sum of the interacting atoms.

In addition, the fingerprint plot enabled us to calculate the percentage contributions of all contacts which are listed in Table S1 (Supplementary data) and shown graphically in Figure 3. It is clear that, the most dominant contacts are H…H, H…C, C…C,

Table III — Hydrogen-bond geometry (Å, º)

D—H···*A*	*D*—H	H···*A*	*D*···*A*	*D*—H···*A*
N3*A*—H3*NA*···O1*A*	0.87 (3)	2.11 (3)	2.795 (2)	136 (2)
N3*B*—H3*NB*···O1*B*	0.86 (3)	2.12 (3)	2.797 (2)	135 (3)
N1*B*—H1*NB*···O1*C*^{vi}	0.94 (3)	1.97 (3)	2.870 (2)	162 (3)
N4*B*—H4*NB*···N2*B*	0.85 (3)	2.22 (3)	2.633 (2)	110 (2)
N4*B*—H4*NB*···O5^{iii}	0.85 (3)	2.23 (3)	2.979 (2)	148 (3)
N4*A*—H4*NA*···N2*A*	0.85 (3)	2.20 (3)	2.630 (2)	111 (2)
N4*A*—H4*NA*···O4^{ii}	0.85 (3)	2.38 (3)	3.159 (3)	153 (2)
N4*C*—H4*NC*···N2*C*	0.83 (3)	2.17 (3)	2.617 (2)	114 (2)
N1*A*—H1*NA*···O1*B*^{iv}	0.94 (3)	1.94 (3)	2.818 (2)	157 (3)
N3*C*—H3*NC*···O1*C*	0.86 (3)	2.09 (3)	2.767 (2)	136 (3)
C12*A*—H12*A*···O2*B*^{v}	0.95	2.58	3.420 (3)	148
C15*A*—H15*A*···S1*A*	0.95	2.55	3.216 (2)	128
C15*B*—H15*B*···S1*B*	0.95	2.50	3.177 (4)	129
C15*C*—H15*C*···S1*C*	0.95	2.55	3.209 (2)	127
C20—H20*A*···O5	0.96	2.29	2.736 (5)	107
C20—H20*C*···O3*B*^{vi}	0.96	2.58	3.324 (5)	134
C21—H21*B*···O3*B*^{vi}	0.96	2.56	3.3170 (17)	136

Symmetry codes: (ii) −*x*+1/2, *y*−1/2, −*z*+3/2; (iii) −*x*, −*y*, −*z*+1; (iv) −*x*+1/2, −*y*+1/2, −*z*+2; (v) −*x*+1/2, −*y*−1/2, −*z*+2; (vi) *x*, −*y*, *z*−1/2.

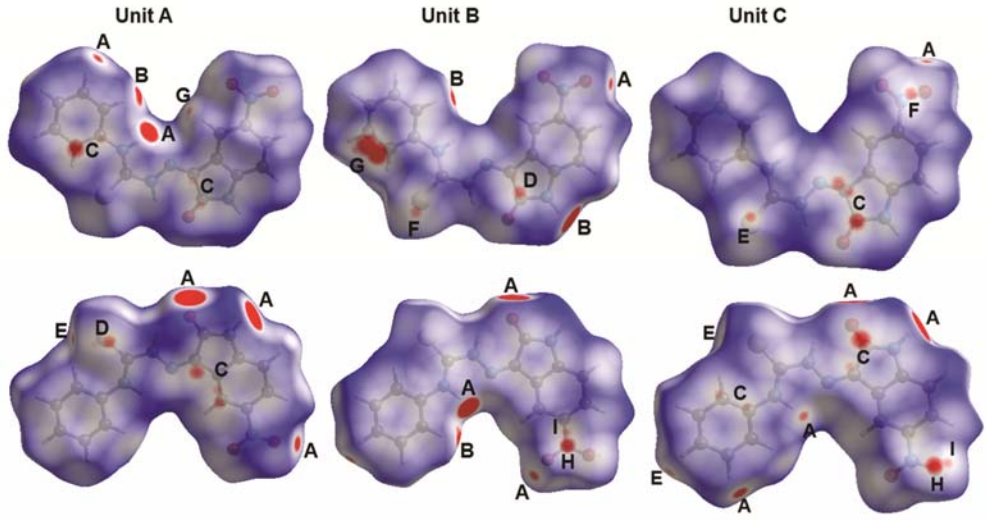

Figure 2 — Hirshfeld d_{norm} surfaces showing the different intermolecular interactions; A: O…H, B: H…H; C: C…C; D: S…C; E: S…H; F: S…N; G: H…C; H: N…O and I: C…O contacts. Units A, B and C refer to the atom numbering in the crystal structure. Units A, B and C refer to the atom numbering in CIF

O…H and S…H interactions. Also, the short contact interactions usually appeared in the fingerprint plots as sharp spikes. This fact is revealed from the decomposed fingerprint plots of the short interactions observed in unit A of the studied compound as an example (Figure 4).

DFT studies

The calculated molecular structure of the ligand as well as the structures overlay between the calculated and experimental one is presented in Figure 5. The Cartesian coordinates of the optimized structure as well as the bond distances and angles compared to the experimental data are given in Table S2 (Supplementary data). It is clear that both structures are very close to each other. There are also good straight line correlations between the calculated and experimental bond distances and angles (Figure 6). The correlation coefficients (R^2) are very close to 1 (0.978-0.980).

The natural charges obtained from the NBO calculations are presented graphically in Figure 7. It is clear that the most electropositive sites are carbon and nitrogen atoms of the carbonyl and nitro groups, respectively. In addition the three NH protons are the most electropositive hydrogen sites. In contrast, the oxygen and nitrogen atoms of the carbonyl and NH groups, respectively, as well as the oxygen atoms of the nitro group are the most electronegative. The S and the majority of carbon atoms have electronegative nature. Only carbon atoms bonded to O, N or S atomic sites have positive natural charges. As a result of this charge distribution, the compound is polar and has a net dipole moment of 3.2962 Debye.

Presentation of electron density mapped over molecular electrostatic potential (MEP) showing the dipole moment vector is presented in Figure 8. The red and blue areas represent the most electron rich and electron poor sites which are in good agreement with the natural charge population analysis. In addition, the red regions are the best candidates as hydrogen bond acceptor sites while the blue regions are the most suited as hydrogen bond donor. The results are also in good agreement with the hydrogen bonding interaction sites observed from the reported X-ray structure analysis.

In addition, the HOMO and LUMO frontier molecular orbitals are important for the molecule reactivity[38-44]. Their energies were calculated to be -6.1294 and -3.0556 eV, respectively. Hence, the calculated ionization potential (I) and electron affinity (A) are 6.1294 and 3.0556 eV, respectively. Also, the hardness, chemical potential and electrophilicity index are 3.0738, -4.5925 and 3.4308 eV, respectively. Since, the HOMO is located mainly over the thiosemicarbazide S-atom while the LUMO is distributed over most of the π-system. Hence, the HOMO to LUMO excitation represents mainly n-π* transition and the least excitation energy is 3.0738 eV.

Table IV — Summary of the intermolecular interactions and the corresponding shortest interaction distances (Å)

Contact	Distance	Contact	Distance
O1A…H1NC	1.856	H11A…H16A	1.955
O1B…H1NA	1.868	H11B…H20A	1.984
O2A…H12C	2.403	H11B…H19A	2.199
O1C…H1NB	1.897	C8A…C15C	3.355
O2B…H12A	2.467	C10C…C7A	3.359
O5…H4NB	2.093	C7A…C8C	3.262
O5…H11B	2.53	C6A…C7C	3.339
O3B…H20C	2.495	C5A…C7C	3.311
O3B…H21B	2.476	C8C…C15A	3.228
O4…H4NC	2.504	C7C…C10A	3.355
O2C…H20B	2.527	S1A…C7B	3.466
H11A...C16	2.654	S1A…C8B	3.402
H5AA...C16	2.711	S1B…N5C	3.267
H20A...C14B	2.749	O2C…N5B	2.918
H20C...C14B	2.728	O2C…C4B	3.167
H15B…C10C	2.759	O2B…C4C	3.21
S1C…H16A	2.811		
S1C…H13A	2.833		
S1A…H13B	2.758		
S1B…H13C	2.796		
S1C…H2B	2.88		

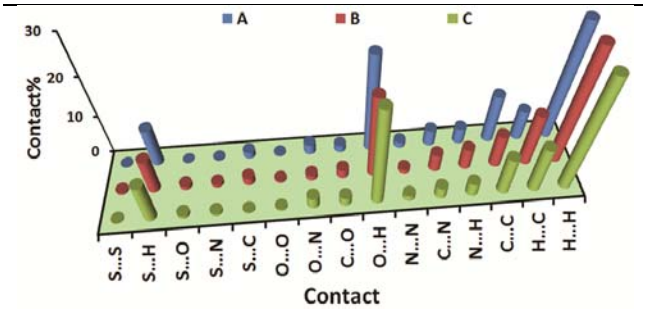

Figure 3 — Summary of the intermolecular interactions

NBO analysis

The electron delocalization processes *via* conjugation effect are important for stabilizing molecular systems[45,46]. In this regard, the different electron delocalization processes and their stabilization energies ($E^{(2)}$) were calculated with the aid of NBO calculations

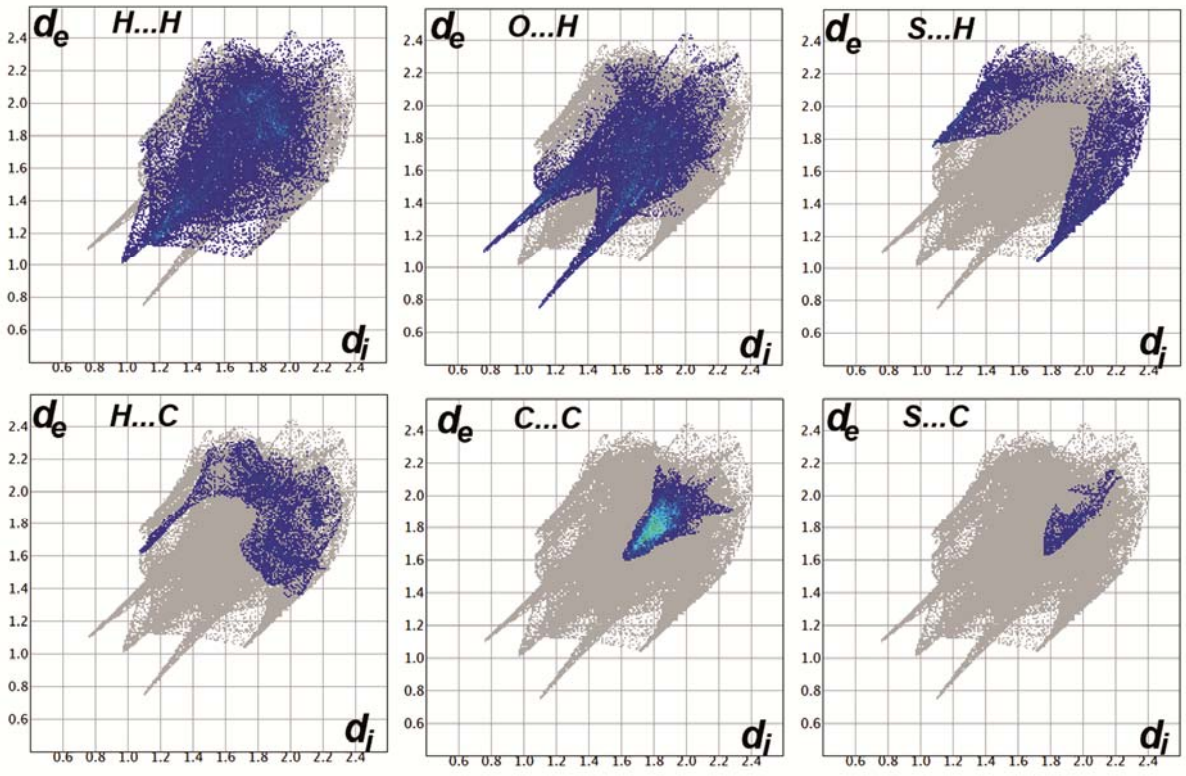

Figure 4 — Decomposed fingerprint plots of the important interactions in unit A

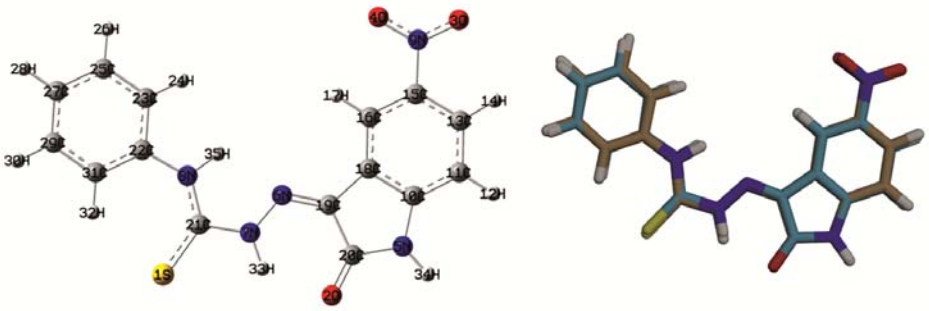

Figure 5 — The optimized geometry (left) and overlay of the optimized with experimental structures (right)

(Table V). These values represent the stabilization energies due to the electron delocalization processes. Different σ-σ*, π→π*, n→σ*, and n→π* electron delocalization processes were found to stabilize the system up to 6.04, 25.57, 27.87 and 162.52 kcal/mol, respectively for BD(1)C11-C13→ BD*(1)N5-C10, BD(2)C13-C15→ BD*(2)O3-N9, LP(2)O2→ BD*(1)N5-C20 and LP(3)O4→ BD*(2)O3-N9. Generally, the n→σ* and σ→σ* electron delocalization processes are the weakest and hence stabilize the molecular system to lower extent compared to π→π* and n→π* ones.

UV-Vis spectra

The experimental UV-Vis electronic spectra of the studied thiosemicarbazide in DMSO showed two spectral bands at 434 and 250 nm. The TD-DFT calculations predicted these electronic transition bands at 430.9 and 257.2 nm, respectively, and their oscillator strength values are 0.1178 and 0.387, respectively. These electronic transitions were assigned to be mainly for HOMO→LUMO (96%) and HOMO→LUMO+2 (90%) excitation, respectively. Presentation of these electronic excitation processes are shown in Figure 9. In agreement with our experimental finding, these electronic spectral bands could be assigned to n-π* and π-π* transitions, respectively.

DNA cleavage studies

The degree to which the compounds could function as DNA cleavage agent was examined using supercoiled pBR322 DNA (0.5 μg/μL) as the target. The efficiency of cleavage of these compounds was investigated through agarose gel electrophoresis using different concentrations of compounds in 1% DMSO/5 mM Tris-HCl/50 mM NaCl buffer at *p*H 7.2, with and without H_2O_2, and with 2 h incubation. The activity of the compounds was estimated by the conversion of DNA from Form I to Forms II and III. The fastest migration is detected in the super coiled form (Form I). If only one strand is cleaved, the supercoils relax to convert into a slower-moving form (Form II). If both strands are cleaved, a linear form (Form III) is produced, which migrates between Forms I and Form II[47].

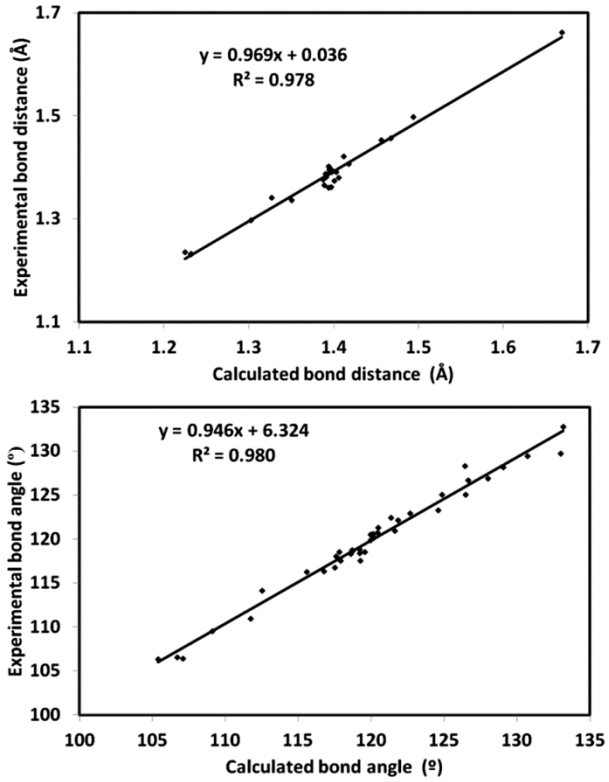

Figure 6 — The straight line correlations between the calculated and experimental geometric parameters

This experiment was evaluated in the presence of H_2O_2 as an oxidizing agent. The control experiment did not show any apparent cleavage of DNA (lane 2). In the presence of the compounds [Schiff base ligand, Ni(II) and Pd(II) complexes] at different concentrations (lanes 4 to 12), the plasmid DNA was converted from Form I to Form II at 1.0 mM (lane 4 for Schiff base ligand; Figure 10).

At 0.4 mM (lane 7), the DNA supercoiled was converted from Form I to Forms II and III (Figure 11; Ni-complex) and at (lane 12), 1.0 mM (Figure 12; Pd-complex).

To investigate the mechanism of DNA cleavage promoted by these compounds, the reactions were allowed to proceed in the presence of DMSO (lane 3) as hydroxyl radical scavengers[48]. The addition of hydroxyl radical scavenger completely inhibits DNA cleavage activity (Schiff base ligand and Ni(II) complex, lane 3), which is induced by these compounds (except for Pd(II) complex). This

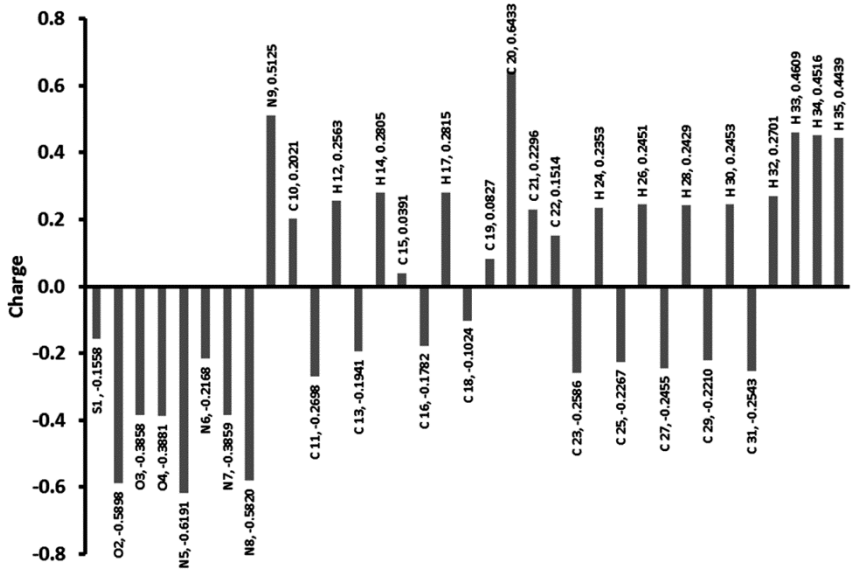

Figure 7 — Natural atomic charges of the ligand; atom numbering refer to Fig. 5

Table V — The $E^{(2)}$ (kcal/mol) values for the charge transfer interactions[a]

Donor NBO	Acceptor NBO	$E^{(2)}$	Donor NBO	Acceptor NBO	$E^{(2)}$
BD(1)C11-C13	BD*(1)N5-C10	6.04	BD(2)O3-N9	BD*(2)O3-N9	7.59
BD(1)C15-C16	BD*(1)C18-C19	5.11	BD(2)N6-C19	BD*(2)O2-C20	13.99
BD(1)C29-C31	BD*(1)N8-C22	5.12	BD(2)N6-C19	BD*(2)C16-C18	10.03
LP(2)S1	BD*(1)N7-C21	11.18	BD(2)C10-C11	BD*(2)C13-C15	24.05
LP(2)S1	BD*(1)N8-C21	11.09	BD(2)C10-C11	BD*(2)C16-C18	15.40
LP(2)O2	BD*(1)N5-C20	27.87	BD(2)C13-C15	BD*(2)O3-N9	25.57
LP(2)O2	BD*(1)N7-H33	6.28	BD(2)C13-C15	BD*(2)C10-C11	15.52
LP(2)O2	BD*(1)C19-C20	18.58	BD(2)C13-C15	BD*(2)C16-C18	22.50
LP(2)O3	BD*(1)O4-N9	19.25	BD(2)C16-C18	BD*(2)N6-C19	19.55
LP(2)O3	BD*(1)N9-C15	12.54	BD(2)C16-C18	BD*(2)C10-C11	22.41
LP(2)O4	BD*(1)O3-N9	19.15	BD(2)C16-C18	BD*(2)C13-C15	17.47
LP(2)O4	BD*(1)N9-C15	12.46	BD(2)C22-C31	BD*(2)C23-C25	18.75
LP(1)N6	BD*(1)N7-H33	8.96	BD(2)C22-C31	BD*(2)C27-C29	20.32
LP(1)N6	BD*(1)N8-H35	6.13	BD(2)C23-C25	BD*(2)C22-C31	20.03
LP(1)N6	BD*(1)C19-C20	12.40	BD(2)C23-C25	BD*(2)C27-C29	17.80
			BD(2)C27-C29	BD*(2)C22-C31	19.83
			BD(2)C27-C29	BD*(2)C23-C25	21.99
			LP(3)O4	BD*(2)O3-N9	162.52
			LP(1)N5	BD*(2)O2-C20	58.17
			LP(1)N5	BD*(2)C10-C11	40.47
			LP(1)N7	BD*(2)S1-C21	56.85
			LP(1)N7	BD*(2)N6-C19	44.63
			LP(1)N8	BD*(2)S1-C21	85.28
			LP(1)N8	BD*(2)C22-C31	33.67

[a]Atom numbering refer to **Fig. 5**

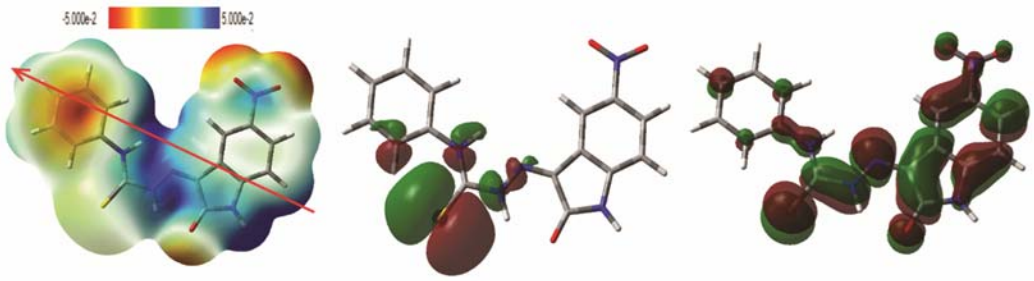

Figure 8 — The MEP, HOMO and LUMO presentation of the ligand

observation suggests the involvement of the hydroxyl radical in the cleavage, thereby confirming the oxidative pathways of these compounds toward DNA[49,50]. In case of Pd(II) complex the supercoiled DNA was completely degraded. These observations suggest that, this complex may be capable of promoting DNA cleavage through both oxidative and hydrolytic DNA damage pathways[51].

The results of cleavage experiments revealed that the Ni(II) complex has more cleavage activity than the Pd(II) complex; probably this may be due to the presence of Ni ion.

Molecular Docking

To conjecture the interaction between the ligand and its metal complexes with DNA, the molecular

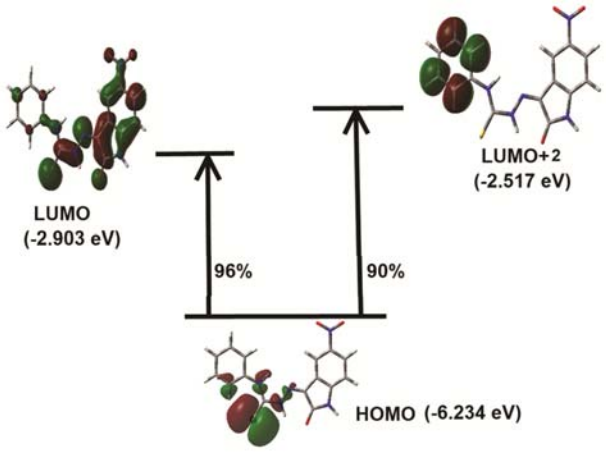

Figure 9 — Presentation of the molecular orbitals included in the electronic transitions of the studied compound in DMSO as solvent

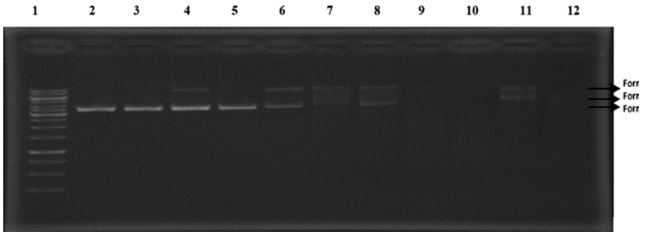

Figure 10 — Cleavage of supercoiled pBR322 (0.5 μg/μL) at different concentrations of Schiff base ligand in Tris-HCl buffer *p*H (7.2) for 2 h at 37°C. Lane 1: DNA ladder; lane 2: DNA + H_2O_2; lane 3: DNA + Schiff base ligand + DMSO; lane (4-12): DNA with increasing the concentrations of Schiff base ligand (1-6 mM) + H_2O_2 + Buffer

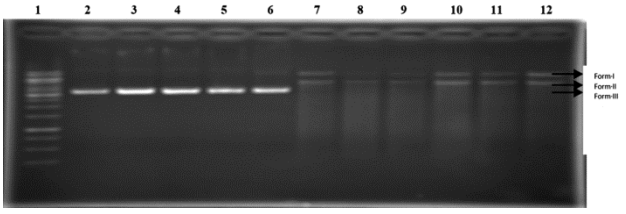

Figure 11 — Cleavage of supercoiled pBR322 (0.5 μg/μL) at different concentrations of Ni(II) complex in Tris-HCl buffer *p*H (7.2) for 2 h at 37°C. Lane 1: DNA ladder; lane 2: DNA + H_2O_2; lane 3: DNA + Ni(II) complex (1 mM) + DMSO; Lanes: (4-12), DNA with increasing the concentrations of Ni(II) complex (0.1 to 1 mM)+ H_2O_2 + Buffer

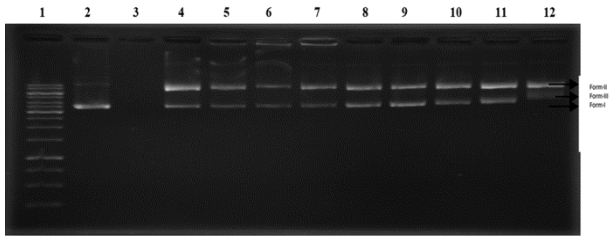

Figure 12 — Cleavage of supercoiled pBR322 (0.5 μg/μL) at different concentrations of Pd(II) complex in Tris-HCl buffer *p*H (7.2) for 2 h at 37°C. Lane 1: DNA ladder; lane 2: DNA + H_2O_2; lane 3: DNA + Pd(II) complex (1mM) + DMSO; Lanes: (4-12), DNA with increasing the concentrations of Pd(II) complex (0.1-1mM) + H_2O_2 + Buffer

docking technique is a suitable mechanism to get the insight of the arbitrary study, by assigning the ligand d and its complexes into the binding site of the DNA. In our research, semi rigid molecular docking (the DNA only was treated as rigid body) studies were performed by MOE software[52,53] to prophesy the binding modes of the ligand and its complexes with a DNA duplex of sequence "d(CGCAAATTTCGC)2" dodecamer (PDB ID: 1BNA), and implement an energetically favourable docked structures (Figure 13). We can observe from the figure that this

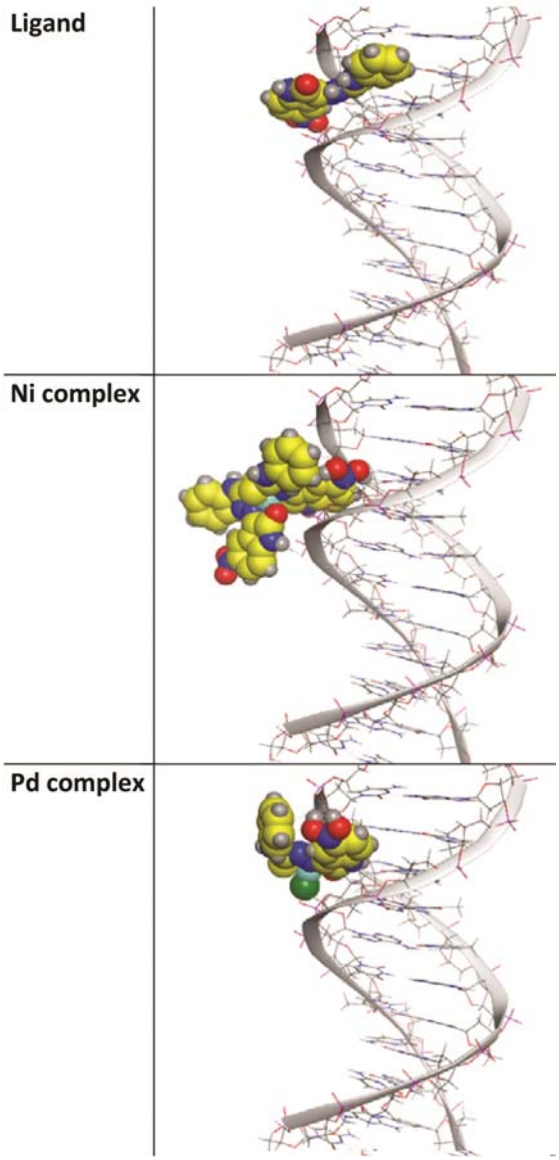

Figure 13 — 3D docking interaction between the ligand, Ni and Pd complexes with 1BNA

ligand and its complexes get attached with DNA throughout minor groove and their moiety shows intercalation between the nucleotide base pairs of DNA as shown in Figure 13. The docked complex of ligand and DNA (Figure 14) represents that the S atom (of thio-ketone group) of the ligand forms a hydrogen bond with the 2nd nitrogen of both guanine of DNA (dG 10(A) and dG16(B)). Where Ni(II) and Pd(II) complexes perform more hydrogen bonds and hydrogen π-staking toward the double helix in the minor groove as shown in Figure 13 and Table VI.

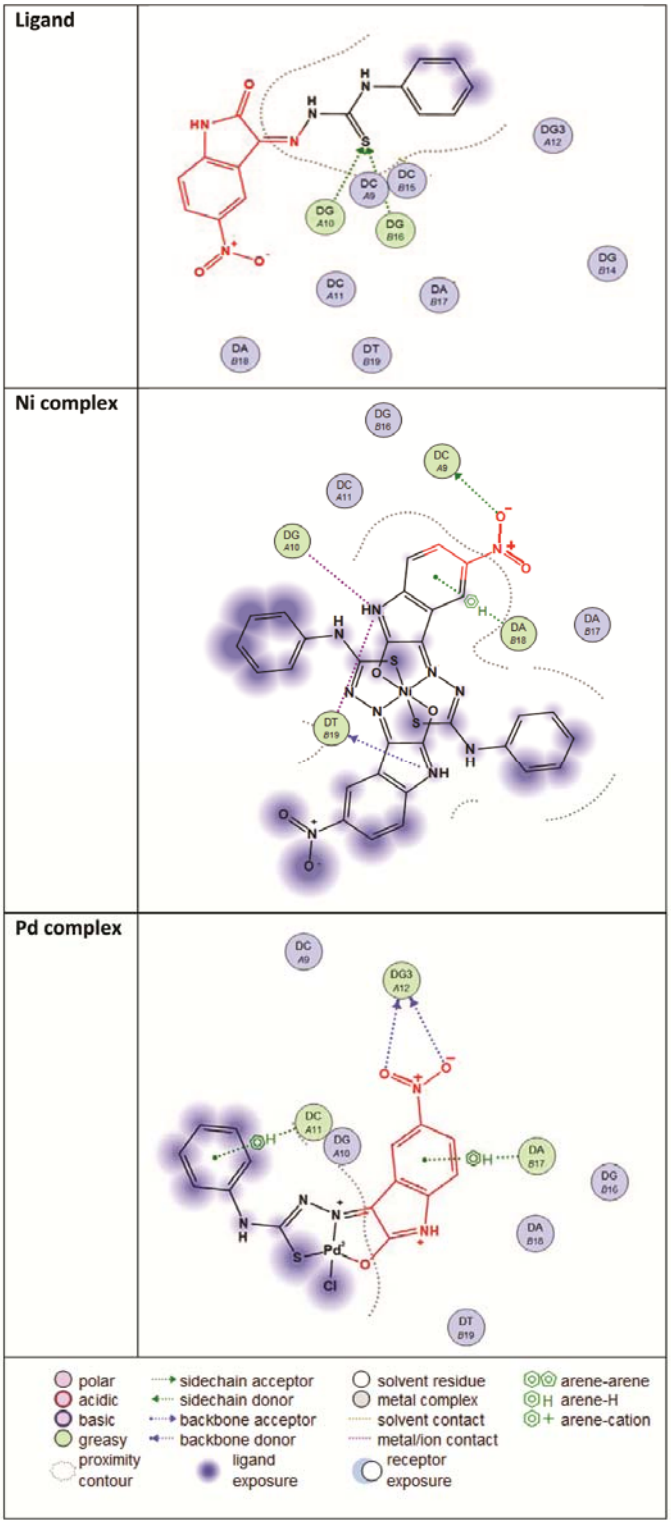

Figure 14 — 2D docking interaction between the ligand, Ni and Pd complexes with 1BNA

The docking score of the ligand and its metal complexes refer to high impact of Ni(II) complex toward the DNA than Pd(II) and the ligand and are – 19.91, -14.62 and -14.17, respectively, as shown in Table VII.

Table VI — Interaction between the ligand, Ni and Pd complexes site complex with 1BNA

Compound	Ligand	Receptor	Interaction	Distance E (Å)	(kcal/mol)
Ligand	S1B 1	N2 DG 10 (A)	H-acceptor	3.53	-1.6
	S1B	N2 DG 16 (B)	H-acceptor	3.05	-0.5
	N4 39	OP2 DT 19 (B)	H-donor	3.08	-3.2
	O 66	O2 DC 9 (A)	H-donor	2.87	-4.2
	6-ring	C4' DA 18 (B)	pi-H	3.52	-0.5
Ni Complex	O 17	O GLY 499 (A)	H-donor	2.92	-1.4
	O 71	OG SER 415 (A)	H-donor	2.93	-1.3
	O 75	OG SER 415 (A)	H-donor	3.20	-0.5
	C 77	SG CYS 498 (A)	H-donor	3.73	-0.8
	O 2	ND2 ASN 418 (A)	H-acceptor	3.16	-1.9
	O 17	N GLY 496 (A)	H-acceptor	2.93	-1.8
	O 83	N CYS 498 (A)	H-acceptor	3.45	-0.9
	5-ring	CA ALA 495 (A)	pi-H	3.72	-0.8
	5-ring	N GLY 496 (A)	pi-H	4.26	-0.9
Pd complex	O 35	OP1 DG3 12 (A)	H-donor	3.42	-1.2
	O 37	OP1 DG3 12 (A)	H-donor	2.96	-4.6
	6-ring	C5' DC 11 (A)	pi-H	4.75	-0.5
	6-ring	C4' DA 17 (B)	pi-H	3.74	-0.6

Table VII — Docking score and energy of between the ligand, Ni and Pd complexes site complex with 1BNA

Compound	S	rmsd_refine	E_conf	E_place	E_score1	E_refine	E_score2
Ligand	-14.62	1.32	68.08	-52.60	-8.71	-134.33	-14.62
	-14.44	0.93	57.80	-48.95	-9.51	-81.94	-14.44
	-13.16	1.09	66.10	-82.11	-9.31	-134.97	-13.16
	-12.27	0.89	66.12	-70.39	-9.88	-134.71	-12.27
	-10.71	1.76	60.93	-48.39	-8.90	-66.68	-10.71
Ni complex	-19.91	1.88	-847.74	-76.30	-17.14	-250.41	-19.91
	-19.00	3.86	-849.32	88.76	-18.81	-255.01	-19.00
	-18.69	5.13	-855.46	64.83	-17.60	-257.64	-18.69
	-18.49	2.92	-852.20	13.90	-19.84	-229.71	-18.49
	-18.01	3.96	-848.94	77.18	-17.31	-239.23	-18.01
Pd complex	-14.17	1.96	-124.43	-19.25	-15.26	-99.60	-14.17
	-13.48	1.19	-122.78	-35.94	-17.01	-169.69	-13.48
	-12.11	0.85	-130.10	-62.79	-15.25	-98.56	-12.11
	-11.83	1.89	-128.29	-80.89	-15.44	-76.99	-11.83
	-11.50	2.01	-129.87	-76.83	-15.29	-69.78	-11.50

Conclusions

Two octahedral Ni(II) and square planar Pd(II) complexes, with a novel tridentate Schiff base ligand have been synthesized and characterized using elemental analyses and various spectroscopic techniques. The O…H, H…H, C…C, S…C, S…H, S…N, H…C, N…O and C…O interactions are the most important contacts based on Hirshfeld calculations. Different electronic parameters of the studied thiosemicarbazide have been calculated at B3LYP/6-31G(d,p) method. The σ-σ*, π→π*, n→σ*, and n→π* processes which stabilize the studied system by conjugation effect have been calculated using NBO method. The UV-Vis spectra of the compound showed two bands at 434 nm (Calc. 430.9 nm) and 250 nm (Calc. 257.2 nm) which could be assigned to HOMO→LUMO (n-π*) and HOMO→LUMO+2 (π-π*) excitations, respectively. Results of gel electrophoresis experiments indicate that these compounds can induce cleavage of plasmid DNA. Cleavage of DNA by these compounds has been found to be concentration dependent. All

compounds show nuclease activity in the presence of oxidant, which may be due to free radical reaction (OH*) with DNA. The docking score of the ligand and its metal complexes refer to high impact for groove binding of Ni(II) complex toward the DNA than Pd(II) and the ligand and are -19.91, -14.62 and -14.17, respectively.

Supplementary Information

Supplementary information is available in the website http://nopr.niscpr.res.in/handle/123456789/58776.

References

1 Aziz T, Rahim F, Ullah R, Ullah A, Haq F, Khan F U, Kiran M, Khattak N S & Iqbal M, *Biomed J Sci Tech Res*, 28 (2020) 21919.

2 Medvedev A, Buneeva O & Glover V, *Biol: Targets Ther,* 1 (2007) 151.

3 Bhardwaj S, Kumar L, Verma R & Singh U K, *J Pharm Res,* 3 (2010) 2983.

4 Chahal V, Nirwan S & Kakkar R, *MedChemComm,* 10 (2019) 351.

5 El-Saied F, El-Aarag B, Salem T, Said G, Khalifa S A M & El-Seedi H R, *Molecules,* 24 (2019) 3313.

6 Hajare R, Kulkarni S, Thakar M & Paranjape R, *World J Pharm Pharm Sci,* 5 (2016) 569.

7 Sharma S, Meena R, Singh R V & Fahmi N, *Main Group Met Chem,* 39 (2016) 31.

8 Bulatov E, Sayarova R, Mingaleeva R, Miftakhova R, Gomzikova M, Ignatyev Y, Petukhov A, Davidovich P, Rizvanov A & Barlev N A, *Cell Death Discov,* 4 (2018) 103.

9 Nair M S, Arish D & Joseyphus R S, *J Saudi Chem Soc,* 16 (2012) 83.

10 Gomathi R, Ramu A & Murugan A, *Bioinorg Chem Appl,* 2014 (2014) 215392.

11 Polo-Cerón D, *Bioinorg Chem Appl,* 2019 (2019) 3520837.

12 Bruker, APEX2, SAINT & SADABS, (Bruker AXS Inc, Madison, Wisconsin, USA) 2005.

13 Sheldrick G M, *Acta Cryst,* A71 (2015) 3.

14 Turner M J, McKinnon J J, Wolff S K, Grimwood D J, Spackman P R, Jayatilaka D & Spackman M A 2017 Crystal Explorer17 University of Western Australia http://hirshfeldsurfacenet.

15 a) Frisch M J, Trucks G W, Schlegel H B, Scuseria G E, Robb M A, Cheeseman J R, Scalmani G, Barone V, Mennucci B, Petersson G A, Nakatsuji H, Caricato M, Li X, Hratchian H P, Izmaylov A F, Bloino J, Zheng G, Sonnenberg J L, Hada M, Ehara M, Toyota K, Fukuda R, Hasegawa J, Ishida M, Nakajima T, Honda Y, Kitao O, Nakai H, Vreven T, Montgomery J A Jr, Peralta J E, Ogliaro F, Bearpark M, Heyd J J, Brothers E, Kudin K N, Staroverov V N, Kobayashi R, Normand J, Raghavachari K, Rendell A, Burant J C, Iyengar S S, Tomasi J, Cossi M, Rega N, Millam J M, Klene M, Knox J E, Cross J B, Bakken V, Adamo C, Jaramillo J, Gomperts R, Stratmann R E, Yazyev O, Austin A J, Cammi R, Pomelli C, Ochterski J W, Martin R L, Morokuma K, Zakrzewski V G, Voth G A, Salvador P, Dannenberg J J, Dapprich S, Daniels A D, Farkas O, Foresman J B, Ortiz J V, Cioslowski J & Fox D J, *GAUSSIAN 09, Revision A02*, (Gaussian Inc, Wallingford CT, USA) 2009; b) *GaussView, Version 41*, Dennington R II, Keith T & Millam J, (Semichem Inc, Shawnee Mission, KS) 2007.

16 Reed A E, Curtiss L A & Weinhold F, *Chem Rev,* 88 (1988) 899.

17 Marten B, Kim K, Cortis C, Friesner R A, Murphy R B, Ringnalda M N, Sitkoff D & Honig B, *J Phys Chem,* 100 (1996) 11775.

18 Tannor D J, Marten B, Murphy R, Friesner R A, Sitkoff D, Nicholls A, Ringnalda M, Goddard W A & Honig B, *J Am Chem Soc,* 116 (1994) 11875.

19 Drew H R, Wing R M, Takano T, Broka C, Tanaka S, Itakura K & Dickerson R E, *Proc Natl Acad Sci USA,* 78 (1981) 2179.

20 Alsaeedi M S, Babgi B A, Hussien M A, Abdellattif M H & Humphrey M G, *Molecules,* 25 (2020) 1033.

21 Prasad R N, Mathur M & Upadhyay A, *J Indian Chem Soc,* 84 (2007) 1202.

22 Wile D M, Gingk B A & Suprlnch T, *Can J Chem,* 45 (1966) 469.

23 Lan-Mei C, Jie L, Jin-Can C, Cai-Ping T, Shuo S, Kang-Cheng Z & Liang-Nian J, *J Inorg Biochem,* 102 (2008) 330.

24 Natarajan R & Sivasangu S, *J Serb Chem Soc,* 75 (2010) 773.

25 Kalliopi C S, Franc P, Athanasios N P, Iztok T, Dimitris P K & George P, *J Inorg Biochem,* 105 (2011) 1273.

26 Ramachandran E, Kalaivani P, Prabhakaran R, Zeller M, Bartlett J H, Adero P O, Wagner T R & Natarajan K, *Inorg Chim Acta,* 385 (2012) 94.

27 Sandra S K, Blaga C R, Zoran B T & Slavica B I, *J Serb Chem Soc,* 72 (2007) 975.

28 Ali A Q, Eltayeb N E & Teoh S G, *IUCr Data,* 1 (2016) x160659.

29 Ali A Q, Eltayeb N E, Teoh S G, Salhin A & Fun H K, *Acta Cryst,* E68 (2012) o285.

30 Ali A Q, Eltayeb N E, Teoh S G, Salhin A & Fun H K, *Acta Cryst,* E68 (2012) o2868.

31 Doğan F, Ulusoy M, Öztürk Ö, Kaya İ & Salih B, *J Therm Anal Calorim,* 98 (2009) 785.

32 Malik S, Jain B & Nema B, *Der Chem Sin,* 7 (2016) 14.

33 Hirshfeld F L, *Theor Chim Acta,* 44 (1977) 129.

34 Spackman M A & Jayatilaka D, *Cryst Eng Comm,* 11 (2009) 19.

35 Spackman M A & McKinnon J J, *Cryst Eng Commun,* 4 (2002) 378.

36 Bernstein J, Davis R E, Shimoni L & Chang N–L, *Angew Chem Int Ed,* 34 (1995) 1555.

37 McKinnon J J, Jayatilaka D & Spackman M A, *Chem Comm,* (2007) 3814.

38 Foresman J B & Frisch Æ, *Exploring chemistry with electronic structure methods*, 2nd ed, (Gaussian, Pittsburgh, USA) 1996.

39 Chang R, *Chemistry*, 7th ed, (McGraw-Hill, New York, USA) 2001.

40 Kosar B & Albayrak C, *Spectrochim Acta,* 78 (1996) 160.

41 Koopmans T A, *Physica,* 1 (1933) 104.

42 Parr R G & Yang W, *Density-functional theory of atoms and molecules*, (Oxford University Press, New York, USA) 1989.

43 Parr R G, Szentpaly L V & Liu S, *J Am Chem Soc,* 121 (1999) 1922.
44 Singh R N, Kumar A, Tiwari R K, Rawat P & Gupta V P, *J Mol Strut,* 1035 (2013) 427.
45 Hubert Joe I, Kostova I, Ravikumar C, Amalanathan M & Pînzaru S C, *J Raman Spectrosc,* 40 (2009) 1033.
46 Sebastian S & Sundaraganesan N, *Spectrochim Acta Part A Mol Biomol Spectrosc,* 75 (2010) 941.
47 Lan J & Pin Y, *Microchem J,* 58 (1998) 144
48 Arjmand F, Parveen S, Afzal M, Toupet L & Ben Hadda T, *Eur J Med Chem,* 49 (2012) 141.
49 Mahalakshmi N & Rajavel R, *Asian J Biochem Pharm Res,* 1 (2011) 525.
50 Ng C H, Ong H K A, Kong C W, Tan K W, Abd Rahman R N Z R, Yamin B M & Ng SW, *Polyhedron,* 25 (2006) 3118.
51 Li D D, Huang F P, Chen G J, Gao C Y, Tian J L, Gu W, Liu X, Yan S P, *J Inorg Biochem,* 104 (2010) 431.
52 Hosny N M, Belal A, Motawea R, Hussien M A & Abdel-Rhman M H, *J Mol Struct,* 1232 (2021) Article 130020.
53 Sharfalddin A A, Emwas A H, Jaremko M & Hussien M A, *Appl Organomet Chem,* 35 (2021) e6041.